Advanced Mathematical Models & Applications
Vol.10, No.1, 2025, pp.144-159
https://doi.org/10.62476/amma101144

EFFECT OF POROUS MEDIUM TO FLUID FLOW IN MUCUS LAYER

Surachai Phaenchat, Kanognudge Wuttanachamsri*

Department of Mathematics, King Mongkut's Institute of Technology Ladkrabang, Bangkok, Thailand

Abstract. Mucociliary clearance (MCC) is a protective process in human respiratory system to expel inhaled strange particles such as dust, dirt, and smoke out of the human body. The particles are caught by mucus residing in the respiratory tract and then mucus forms a mucus layer (ML) lining above the cilia settling on the ciliated epithelial cells. The mucus is removed from the human body by ciliary beating. Here, we study the fluid flow above the tips of cilia up to the mucus layer affected by the movement of cilia. In this work, the two-dimensional Stokes equation is applied to find the velocities of the fluid in the free-fluid region. The numerical solutions are approximated by using a mixed finite element method. This problem can be usefully applied to problems in which fluids are affected by the self-movement of a solid phase.

Keywords: Stokes equation, mixed finite element method, free-fluid region, mucus layer.
AMS Subject Classification: 35Q35, 35Q90, 35Q92, 65N30, 76D07, 76Z05, 76Z10, 92B05.
Corresponding author: Kanognudge Wuttanachamsri, Department of Mathematics, King Mongkut's Institute of Technology Ladkrabang, Ladkrabang, Bangkok 10520, Thailand, e-mail: *kanognudge.wu@kmitl.ac.th*
Received: 20 May 2024; Revised: 28 July 2025; Accepted: 16 September 2025; Published: 10 April 2025.

1 Introduction

Mucus is a viscous fluid produced in the human body, in which the mucus comprises of 95% water, 2–3% glycoproteins and proteins, 1% mineral, 1% lipids and 0.02% DNA (Matthews et al., 1963; Potter et al., 1967). The mucus is part of airway surface liquid (ASL) that lines between the epithelial cells and air in the respiratory tract. The ASL consists of two layers: the mucus layer (ML) and the periciliary layer (PCL). The mucus layer is adjacent to the air surface and is on the PCL covering the epithelial cell surface (Boucher, 1999; Derichs et al., 2011) as shown in Figure 1. Figure 1 shows a portion of a cross-section of the trachea that comprises of the inhaled particles, air, the mucus layer (ML), the periciliary layer (PCL), cilia, epithelial cells, ciliated cells and goblet cells. The PCL consists of two phases: liquid and solid phases, where the liquid and solid phases are the PCL fluid and cilia, respectively. Therefore, the PCL is considered as a porous medium. The mucus is secreted from the goblet cell scattering in the epithelial cell to catch foreign particles that get into the human body. After that the mucus forms the mucus layer lining above the PCL and is moved out of the body by the beating of cilia. This mechanism is called Mucociliary clearance (MCC), which is the primary innate defense mechanism of the human respiratory system (Knowles & Boucher, 2002; Wanner et al., 1996).

How to cite (APA): S. Phaenchat, K. Wuttanachamsri (2025). Effect of porous medium to fluid flow in mucus layer. *Advanced Mathematical Models & Applications*, *10*(1), 144-159 https://doi.org/10.62476/amma101144

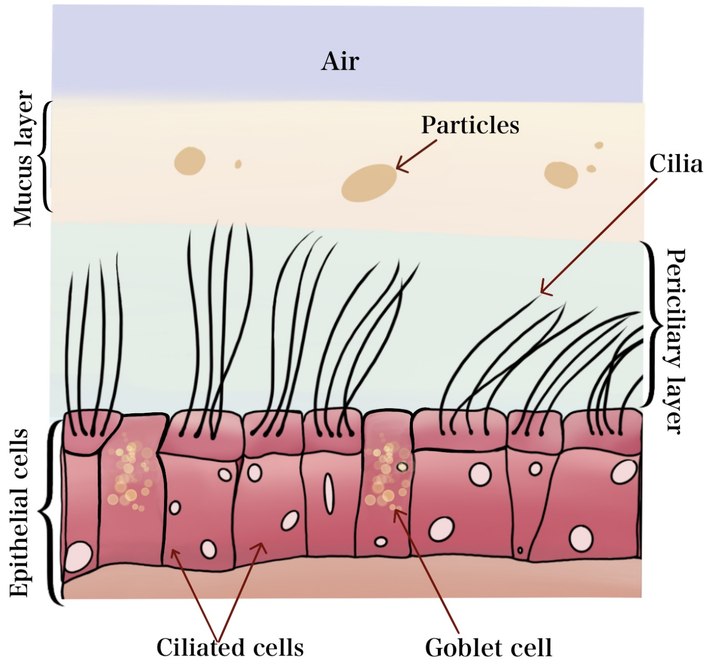

Figure 1: The clearance of mucus in the respiratory system

Several studies investigated MCC both numerically and experimentally (Battle et al., 2015; Ding et al., 2014; Houtmeyers et al., 1999; Lale et al., 1998; Rusznak et al., 1994; Satir & Christensen, 2007; Sedaghat et al., 2023; Vanaki et al., 2020; Xu & Jiang, 2015). For example, Xu & Jiang (2015) considered five rods (cilia) for both symmetric and asymmetric cilia motion by using a rod-propel-fluid model. They found that the cilium height difference was efficient in driven transport and the transport capacity of the MCC increased when cilia density and cilia beating frequency increased. Ding et al. (2014) studied the fluid flow in both the PCL and the ML by using three-dimensional microscale equations. Sedaghat et al. (2023) studied the effect of cilia abnormalities on mucociliary clearance (MCC) in bronchial airways by using three-dimensional incompressible modified Navier-Stokes equations. The finite difference projection method was used to solve these equations. Vanaki et al. (2020) investigated the cilia in both the healthy state and the disease state for mucociliary clearance in the human respiratory system. They found the numerical solutions depending on various parameters such as ciliary beat frequency (CBF), metachronal waves of cilia, surface tension at the PCL-mucus interface, ciliary length, ciliary density, and liquid depth in the airway. Poopra & Wuttanachamsri (2019, 2022) and SuanKasem et al. (2018) studied the velocity of the PCL fluid using one-dimensional Stokes-Brinkman equations by using asymptotic expansion method in different approaches. Phaenchat & Wuttanachamsri (2019), and Kasamwan & Wuttanachamsri (2020) calculated the velocities of PCL fluid by using a finite element method, a finite different method and classical linearization method. Chamsri (2014) used a mixed finite element method to discretize the n-dimensional macroscale Stokes-Brinkman equations which were used to find the velocity of the PCL fluid in Wuttanachamsri & Schreyer (2020). Free interfaces at the tips of cilia in the PCL was presented in Wuttanachamsri (2020). Verma & Rana (2015) used steady-state mathematical model to study mucus transport in the airway in the human lung. Modaresi & Shirani (2023) investigated the velocities of both the PCL and ML by using three-dimensional mathematical models. The velocities were influenced by variations in mucus viscosity and distinct velocities at the PCL/ML interface. Wuttanachamsri et al. (2024) provided the velocity of the PCL fluid in the porous medium when cilia beat forward by using the two-dimensional Brinkman equation.

Here, we examine the velocity profiles of both the PCL fluid and the mucus. Figure 2 depicts the computational domain used in our investigation, which consists of the ML and the

PCL. Within the PCL, the black straight lines represent cilia, which make the angle θ with the horizontal plane. The variable y_{PCL} is the y value at the interface between the PCL and the ML and y_{in} is y value at the interface between the porous medium and the free-fluid region. For example, the symbols $y_{in}(80^\circ)$ and $y_{in}(70^\circ)$ are y values at the interface between the porous medium and the free-fluid region when cilia make the angle 80° and 70° with the horizontal plane, respectively. When cilia make an angle $\theta < 90^\circ$, the PCL can be divided into two layers: the porous medium, comprising both the PCL fluid and cilia, and the free-fluid region, containing only the PCL fluid. For $\theta = 90^\circ$, there exists only the porous medium in the PCL. In this work, we concentrate on two domains: the free-fluid region, Ω_1, and the ML, Ω_2. In domain Ω_1, the free-fluid region occurs at the angle $\theta < 90^\circ$. As cilia bend downward to various angles, the height of the free-fluid region varies from y_{in} to y_{PCL}. For example, at the angle 80°, the height from $y_{in}(80^\circ)$ to y_{PCL} is 0.0152, while at the angle 70°, the height from $y_{in}(70^\circ)$ to y_{PCL} is 0.0603.

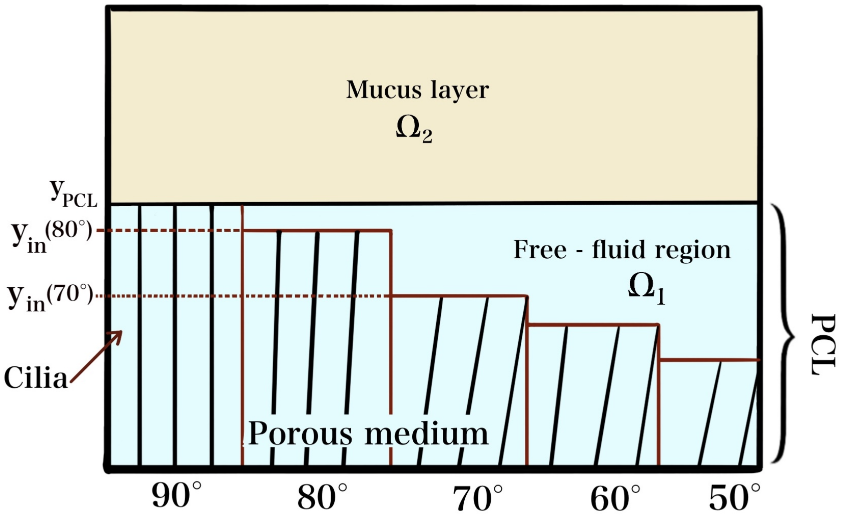

Figure 2: Cartoon picture of the PCL and the ML

To determine the velocities of the fluids in Ω_1 and Ω_2 influenced by cilia movement, we use the velocity of the PCL fluid within the porous medium obtained from Wuttanachamsri et al. (2024) as the lower boundary condition of domain Ω_1 to compute the velocity of the PCL fluid in Ω_1. After that, we adopt the velocity of the PCL fluid within Ω_1 as the lower boundary condition of domain Ω_2 to determine the velocity of the mucus. By creating the numerical domain in which the self-movement of cilia affects the fluid flow in domains Ω_1 and Ω_2 when cilia make various angles to the horizontal plane within one numerical domain, and the fluid velocity in Ω_1 is used to calculate the mucus velocity, to the author's knowledge, this research has never been done before. In this work, the velocities of the fluids in Ω_1 and Ω_2 are found by using the two-dimensional Stokes equation. A mixed-finite element method is used to approximate the numerical solutions.

In Section 2, we present the governing equation. The discretization of the mathematical model using a mixed-finite element method is described in Section 3. The numerical results of the velocities of the fluid in Ω_1 and Ω_2 are presented in Section 5. The conclusion is drawn in Section 6.

2 Governing Equation

In this section, we provide the governing equation used in this work. We assume that the fluids in Ω_1 and Ω_2 moving past the layers are incompressible. Therefore, we use the Stokes equation and the continuity equation in both domains,

$$\nabla p - \mu \Delta \mathbf{v} = \rho \mathbf{g}, \tag{1}$$

$$\nabla \cdot \mathbf{v} = 0, \tag{2}$$

where μ is a dynamic viscosity, p is pressure, ρ is fluid density, $\mathbf{v}$ is velocity of the fluid and $\mathbf{g}$ is gravity. In the two-dimensional domain, let $\mathbf{v} = (u, v)$ and $\mathbf{g} = (g_x, g_y)$. Then Eqs. (1) and (2) can be rewritten as

$$\frac{\partial p}{\partial x} - \mu\left(\frac{\partial^2 u}{\partial x^2} + \frac{\partial^2 u}{\partial y^2}\right) = \rho g_x, \tag{3}$$

$$\frac{\partial p}{\partial y} - \mu\left(\frac{\partial^2 v}{\partial x^2} + \frac{\partial^2 v}{\partial y^2}\right) = \rho g_y, \tag{4}$$

$$\frac{\partial u}{\partial x} + \frac{\partial v}{\partial y} = 0. \tag{5}$$

We now have three equations and three unknowns, which are u, v and p. The governing equations (3) - (5) will be discretized in the next section.

3 Model Discretization

The mathematical model in Section 2 is discretized in this section by using a mixed finite element method. Define w and Q be quadratic and linear weight functions. To find the weak formulation, we multiply Eqs. (3) - (4) by w and Eq. (5) by Q and integrate over the domain Ω_i, $i = 1, 2$. Then Eqs. (3) - (5) becomes

$$\int_{\Omega_i} \left[w\frac{\partial p}{\partial x} - \mu w \left(\frac{\partial^2 u}{\partial x^2} + \frac{\partial^2 u}{\partial y^2}\right)\right] d\Omega_i = \int_{\Omega_i} \rho g_x w \, d\Omega_i, \tag{6}$$

$$\int_{\Omega_i} \left[w\frac{\partial p}{\partial y} - \mu w \left(\frac{\partial^2 v}{\partial x^2} + \frac{\partial^2 v}{\partial y^2}\right)\right] d\Omega_i = \int_{\Omega_i} \rho g_y w \, d\Omega_i, \tag{7}$$

$$\int_{\Omega_i} \left[Q\left(\frac{\partial u}{\partial x} + \frac{\partial v}{\partial y}\right)\right] d\Omega_i = 0. \tag{8}$$

Applying Green's identity to the left-hand side of Eq. (6) and (7), we have

$$\begin{aligned}\int_{\Omega_i} \left[\mu\left(\frac{\partial w}{\partial x}\frac{\partial u}{\partial x} + \frac{\partial w}{\partial y}\frac{\partial u}{\partial y}\right) - \frac{\partial w}{\partial x} p\right] d\Omega_i &= \int_{\Omega_i} \rho g_x w \, d\Omega_i \\ + \int_{\Gamma_i} \left[\mu w \left(\frac{\partial u}{\partial x} n_x + \frac{\partial u}{\partial y} n_y\right) - w p n_x\right] d\Gamma_i,\end{aligned} \tag{9}$$

$$\begin{aligned}\int_{\Omega_i} \left[\mu\left(\frac{\partial w}{\partial x}\frac{\partial v}{\partial x} + \frac{\partial w}{\partial y}\frac{\partial v}{\partial y}\right) - \frac{\partial w}{\partial y} p\right] d\Omega_i &= \int_{\Omega_i} \rho g_y w \, d\Omega_i \\ + \int_{\Gamma_i} \left[\mu w \left(\frac{\partial v}{\partial x} n_x + \frac{\partial v}{\partial y} n_y\right) - w p n_y\right] d\Gamma_i,\end{aligned} \tag{10}$$

where n_x and n_y are outward unit normal vectors in $x-$ and $y-$directions, respectively. Let V_h and P_h be finite-dimensional subspaces of $H^1(\Omega)$ and $L_0^2(\Omega)$, respectively, where $L_0^2(\Omega) = \{p \in$

$L^2(\Omega) : \int_\Omega p \, d\Omega = 0\}$. Let $(u, v, p) \in V_h \times V_h \times P_h$ and the variables u, v and p be expressed as

$$u(\mathbf{x}) = \sum_{n=1}^{N} \psi_n(\mathbf{x}) u^n = \psi^T \mathbf{U}, \tag{11}$$

$$v(\mathbf{x}) = \sum_{n=1}^{N} \psi_n(\mathbf{x}) v^n = \psi^T \mathbf{V}, \tag{12}$$

$$p(\mathbf{x}) = \sum_{l=1}^{L} \phi_l(\mathbf{x}) p_l = \phi^T \mathbf{P}, \tag{13}$$

where $\mathbf{U}$ and $\mathbf{V}$ are the vectors of the velocities, $\mathbf{P}$ is a vector of the pressure, the superscript T represents the transpose operation. The vectors ψ and ϕ are quadratic and linear shape functions, respectively. Let the weight functions w and Q be approximated as

$$w \approx \psi_n, \quad Q \approx \phi_l. \tag{14}$$

Substituting Eqs. (11) - (14) into Eqs. (8) - (10), we have

$$\begin{aligned} &\mu \int_{\Omega_i} \left(\frac{\partial \psi}{\partial x} \frac{\partial \psi^T}{\partial x} + \frac{\partial \psi}{\partial y} \frac{\partial \psi^T}{\partial y} \right) d\Omega_i \mathbf{U} - \int_{\Omega_i} \frac{\partial \psi}{\partial x} \phi^T d\Omega_i \mathbf{P} = \int_{\Omega_i} \rho g_x \psi \, d\Omega_i \\ &+ \mu \int_{\Gamma_i} \left(\psi \frac{\partial \psi^T}{\partial x} n_x + \psi \frac{\partial \psi^T}{\partial y} n_y \right) d\Gamma_i \mathbf{U} - \int_{\Gamma_i} \psi \phi^T n_x \, d\Gamma_i \mathbf{P}, \end{aligned} \tag{15}$$

$$\begin{aligned} &\mu \int_{\Omega_i} \left(\frac{\partial \psi}{\partial x} \frac{\partial \psi^T}{\partial x} + \frac{\partial \psi}{\partial y} \frac{\partial \psi^T}{\partial y} \right) d\Omega_i \mathbf{V} - \int_{\Omega_i} \frac{\partial \psi}{\partial y} \phi^T d\Omega_i \mathbf{P} = \int_{\Omega_i} \rho g_y \psi \, d\Omega_i \\ &+ \mu \int_{\Gamma_i} \left(\psi \frac{\partial \psi^T}{\partial x} n_x + \psi \frac{\partial \psi^T}{\partial y} n_y \right) d\Gamma_i \mathbf{V} - \int_{\Gamma_i} \psi \phi^T n_y \, d\Gamma_i \mathbf{P}, \end{aligned} \tag{16}$$

$$\int_{\Omega_i} \phi \frac{\partial \psi^T}{\partial x} \, d\Omega_i \mathbf{U} + \int_{\Omega_i} \phi \frac{\partial \psi^T}{\partial y} \, d\Omega_i \mathbf{V} = \mathbf{0}. \tag{17}$$

Let $\Omega_i = \bigcup_e \Omega_i^e$, $i = 1, 2$, where Ω_i^e is the element domain. Then Eqs. (15) - (17) can be written in the element matrix form as follows

$$\begin{bmatrix} K & \mathbf{0} & -A_1 \\ \mathbf{0} & K & -A_2 \\ A_1^T & A_2^T & \mathbf{0} \end{bmatrix} \begin{Bmatrix} \mathbf{U} \\ \mathbf{V} \\ \mathbf{P} \end{Bmatrix} = \begin{Bmatrix} F_1 \\ F_2 \\ \mathbf{0} \end{Bmatrix}, \tag{18}$$

where the elements in the coefficient matrix are defined as

$$\begin{aligned} K &= \mu \int_{\Omega_i^e} \left(\frac{\partial \psi}{\partial x} \frac{\partial \psi^T}{\partial x} + \frac{\partial \psi}{\partial y} \frac{\partial \psi^T}{\partial y} \right) d\Omega_i^e, \\ A_1 &= \int_{\Omega_i^e} \frac{\partial \psi}{\partial x} \phi^T d\Omega_i^e, \\ A_2 &= \int_{\Omega_i^e} \frac{\partial \psi}{\partial y} \phi^T d\Omega_i^e, \\ F_1 &= \int_{\Omega_i^e} \rho g_x \psi \, d\Omega_i^e + \mu \int_{\Gamma_i^e} \left(\psi \frac{\partial \psi^T}{\partial x} n_x + \psi \frac{\partial \psi^T}{\partial y} n_y \right) d\Gamma_i^e \mathbf{U} - \int_{\Gamma_i^e} \psi \phi^T n_x \, d\Gamma_i^e \mathbf{P}, \\ F_2 &= \int_{\Omega_i^e} \rho g_y \psi \, d\Omega_i^e + \mu \int_{\Gamma_i^e} \left(\psi \frac{\partial \psi^T}{\partial x} n_x + \psi \frac{\partial \psi^T}{\partial y} n_y \right) d\Gamma_i^e \mathbf{V} - \int_{\Gamma_i^e} \psi \phi^T n_y \, d\Gamma_i^e \mathbf{P}, i = 1, 2. \end{aligned} \tag{19}$$

We now obtain the element matrix form for the domains Ω_1 and Ω_2. The boundary conditions used in this problem are provided in the next section.

4 Boundary Conditions

The boundary conditions used in this research are presented in this section. Figure 3 shows the domains and boundaries used in this study. The variable y_{ML} is the y value at the top of domain Ω_2. Although y_{PCL} is the length of cilia when cilia are perpendicular to the horizontal plane, in this study, we use dimensionless y_{PCL} which is equal to 1. Similarly, we use dimensionless y_{ML}. So y_{ML} is equal to 2. Here, we suppose that cilia bend downward from $\theta = 90°$ to other angles, decreasing by 10° for every 0.2 change in the x-axis. That is, when cilia make the angles $\theta = 90°, 80°, 70°, 60°$ and 50°, they correspond to the ranges of $x = 0$ to $x = 0.2$, $x = 0.2$ to $x = 0.4$, $x = 0.4$ to $x = 0.6$, $x = 0.6$ to $x = 0.8$, and $x = 0.8$ to $x = 1$, respectively. We assume cilia stop beating at the angle $\theta = 40°$ (Sears et al., 2013). The boundary Γ_1 is at the tips of the cilia excluding the case that $\theta = 90°$. The boundary Γ_2 is at the interface between the free-fluid region, Ω_1, and the ML, Ω_2. The boundary Γ_3 is the right boundary of Ω_1. The boundaries Γ_4, Γ_5 and Γ_6 are at the left, right and the top borders of Ω_2, respectively. In this work, we assume that the velocity is continuous at the free-fluid region/the ML interface (at Γ_2).

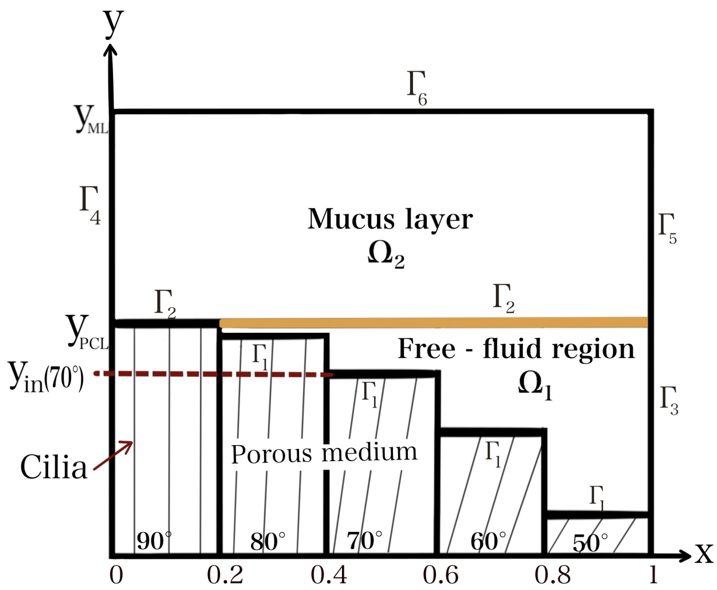

Figure 3: Domains and boundaries.

We first consider the free-fluid region, Ω_1. The velocity of the PCL fluid at Γ_1 is obtained from Wuttanachamsri et al. (2024). That is

$$\begin{aligned} u(x, y_{in}) &= u_{in} \text{ at } \Gamma_1, \\ v(x, y_{in}) &= v_{in} \text{ at } \Gamma_1, \end{aligned} \tag{20}$$

where u_{in} and v_{in} are the velocities of the PCL fluid in $x-$ and $y-$directions at the boundary Γ_1.

For the ML, Ω_2, we use the velocity of the PCL fluid obtained from Ω_1 to be the boundary condition at the bottom of Ω_2. The velocity of the PCL fluid at $y = y_{in}(90°)$ is obtained from Wuttanachamsri et al. (2024). At the boundary Γ_6, we assume that

$$\begin{aligned} \frac{\partial u(x, y_{ML})}{\partial y} &= 0 \text{ at } \Gamma_6, \\ \frac{\partial v(x, y_{ML})}{\partial y} &= 0 \text{ at } \Gamma_6. \end{aligned} \tag{21}$$

The velocities at the boundaries Γ_3, Γ_4 and Γ_5 are unknown. The boundary conditions will be applied to Eq. (18) to find the velocities of the fluids in Ω_1 and Ω_2 in the next section.

5 Numerical Results

In this section, we present the numerical results of the two-dimensional Stokes equation by using a mixed finite element method. To find the velocities of the fluids in Ω_1 and Ω_2, we first provide the velocity of the PCL fluid at the tips of cilia, obtained from Wuttanachamsri et al. (2024), when cilia make the angle $\theta = 90°$ to $50°$ to the horizontal plane. In Wuttanachamsri et al. (2024), the authors have found the velocity of the PCL fluid in the porous domain for the forward stroke of cilia. Figure 4 illustrates the velocity u of the PCL fluid at the tips of cilia at $\theta = 90°, 80°, 70°, 60°$ and $50°$. Note that the velocities decrease when θ decreases. Figure 5 shows the velocity v of the PCL fluid at the tips of cilia. Remark that the velocity v is greater than zero at $\theta = 90°$ and drops to the negative values at other angles. This is because the cilia bend down during their forward stroke. The velocity of the PCL fluid at the tips of the cilia is used to be the bottom boundary condition of Ω_1 (at Γ_1) except the velocity at $\theta = 90°$. This is due to the absence of a free-fluid region in Ω_1 when the cilia are perpendicular to the horizontal plane. The outward unit normal vector $\mathbf{n} = (n_x, n_y)$ used in this work is $(0, -1)$ at Γ_1, $(1, 0)$ at Γ_3 and Γ_5, $(-1, 0)$ at Γ_4 and $(0, 1)$ at Γ_6. At Γ_2, we assume that the velocity is continuous at the free-fluid region / the ML interface.

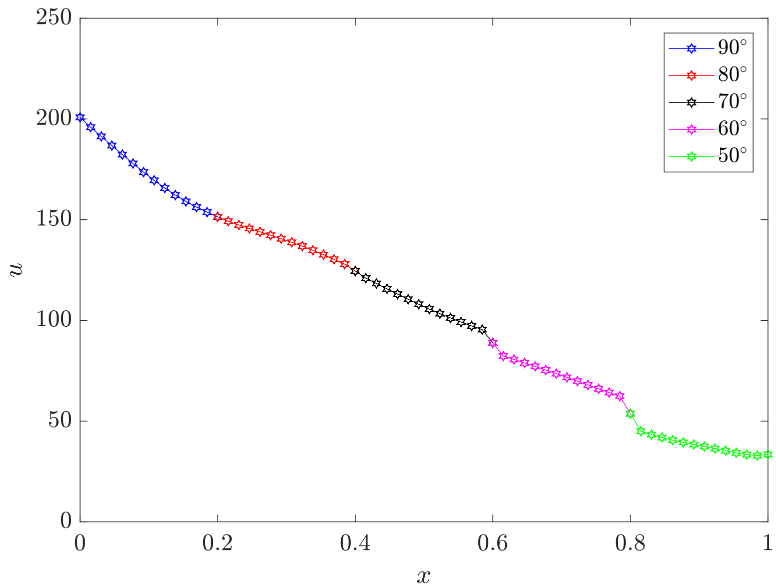

Figure 4: The velocity u of the PCL fluid at the tips of the cilia for each angle

The values of other variables used to calculate the numerical result in the domains Ω_1 and Ω_2 are as follows. The gravity $\mathbf{g} = (0, 9.8 \times 10^{-6})(\mu m/s^2)$ and the fluid density $\rho = 992.2 \times 10^{-15}(g/\mu m^3)$, which is the density of the water at 40°C (The Engineering ToolBox, 2013). Since the viscosity of the PCL fluid and the mucus are different, the viscosities used in this paper are $\mu = 3 \times 10^{-6}(g/(\mu m \cdot s))$ in Ω_1 (Wuttanachamsri & Schreyer, 2020) and $\mu = 2 \times 10^{-5}(g/(\mu m \cdot s))$ in Ω_2 (Chatelin & Poncet, 2016).

The numerical solutions are verified by comparing them with an exact solution (Koplik et al., 1983). The domain of the problem consists of the porous medium below a free-fluid layer and an impermeable plate dragged in the x-direction at the top of the domain. In this work, we only compare our numerical solution with the velocity of free fluid above the porous medium. Since our numerical solution is calculated in the two-dimensional domain, we average the numerical solution over the x-direction and compare the average result with the exact solution. Figure 6 illustrates the average velocities calculated from different mesh refinements which are 5, 11 and 17 nodes in $y-$direction, and the exact solution. It presents that the average velocities converge

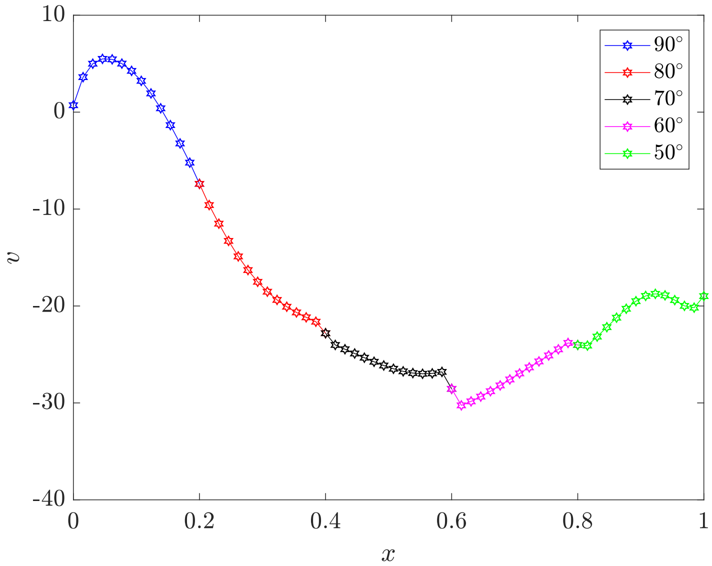

Figure 5: The velocity v of the PCL fluid at the tips of the cilia for each angle

to the exact solution when the number of nodes in y-direction increases. The l_2-norm errors of the average velocities are shown in Table 1. It shows that the error decreases as the number of nodes in $y-$direction increases.

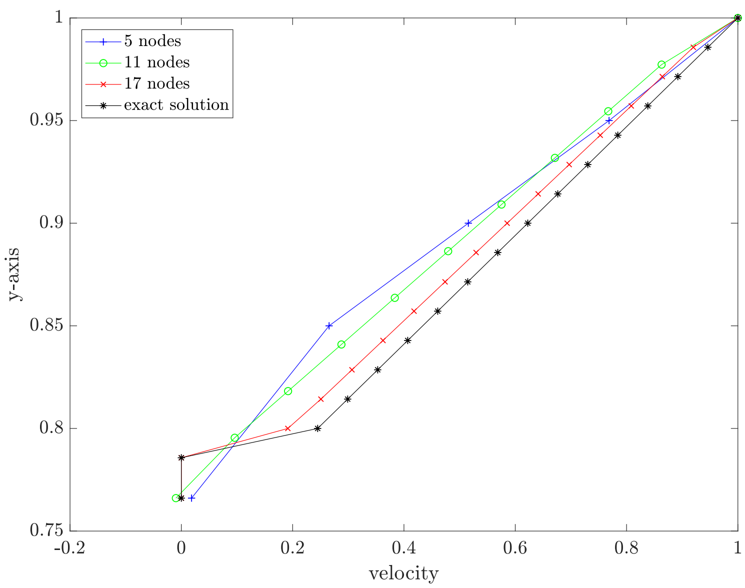

Figure 6: The average velocities for 5, 11 and 17 nodes in y-direction and the exact solution

#nodes in y-direction	l_2-norm errors
5 nodes	0.3047
11 nodes	0.2856
17 nodes	0.1461

Table 1: The l_2-norm errors of the nodes in y-direction

Next, we find the velocities of fluids in Ω_1 and Ω_2 by applying a mixed finite element method to the two-dimensional Stokes equation with the boundary conditions mentioned in the previous section. The number of grid points used in this work is 3051 grid points which is generated by the open software Netgen (Schöberl, 1997). The velocity of the fluid in Ω_1 is provided in Figures 7 and 8 at the angle $\theta = 80^\circ - 50^\circ$. So, the velocity of the fluid in Ω_1 starts at $\theta = 80^\circ$ from $x = 0.2$ to 0.4. For the x ranges of the angle $\theta = 70^\circ, 60^\circ$ and 50° are $x = 0.4$ to 0.6, $x = 0.6$ to 0.8 and $x = 0.8$ to 1, respectively. The heights of domain Ω_1 from $y_{in}(\theta)$ to y_{PCL} for the angle $\theta = 80^\circ, 70^\circ, 60^\circ$ and 50° are $0.0152, 0.0603, 0.1339$ and 0.2339, respectively. Figure 7 shows the velocity u of the fluid in Ω_1 which is highest at $\theta = 80^\circ$ and it decreases when the angle decreases. Figure 8 demonstrates that the velocity v of the fluid in Ω_1 is the negative value when cilia are bending in a downward direction, which the least negative value occurs at $\theta = 60^\circ$. Then the velocity has less negative until $\theta = 50^\circ$.

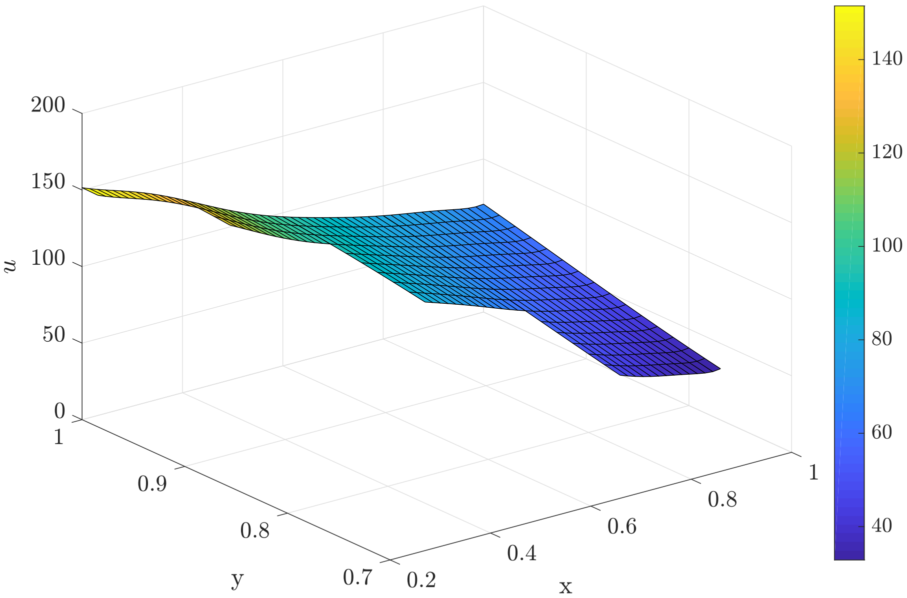

Figure 7: The velocity u of the fluid in Ω_1

To find the velocity of mucus in Ω_2, we use the velocity at the top of the domain Ω_1 to be the velocity at the bottom of the domain Ω_2. The domain Ω_2 is $[0, 1] \times [1, 2]$. Figure 9 shows that the mucus velocity u is maximum at $(x, y) = (0, 1)$ and minimum at $(x, y) = (0.98, 1)$ which is at the bottom boundary of Ω_2. Although, from the left to the right, the velocity u of mucus declines when $y \in [1, 1.4]$ for all x, the velocity u of mucus is almost the same when $y \in [1.4, 2]$ for all x. Therefore most of the mucus moves at a constant velocity in the x-direction. Figure 10 illustrates the velocity v of mucus. Since the velocity v of the mucus is affected by the bottom boundary condition of the velocity v of the fluid in Ω_1, the velocity v is negative and then the velocity v of mucus is significantly more negative when $x \in [0.14, 1]$ for $y \leq 1.4$. The velocity v of mucus fluctuates like a wave but the value does not vary much when $y \geq 1.4$ for all x.

The horizontal velocity of the fluid in Ω_1 (Figure 7) and the mucus velocity (Figure 9) are averaged over the $x-$axis and plotted together in Figure 11. Figure 11 shows the average velocity u of the fluid in Ω_1 and mucus, where the blue diamond and red square refer to the average velocity u of mucus and the fluid in Ω_1, respectively. The average velocity u begins to fluctuate since $y \geq y_{PCL}$ and alternates like a vertical wave. The mean value of the average velocity u is approximately 119 $\mu m/s$. Similarly, the average vertical velocity is illustrated in Figure 12. It shows that the average velocity v is negative and it has less negative when y increases. The velocities u and v in Figures 11 and 12 are employed to find the speeds of the PCL fluid

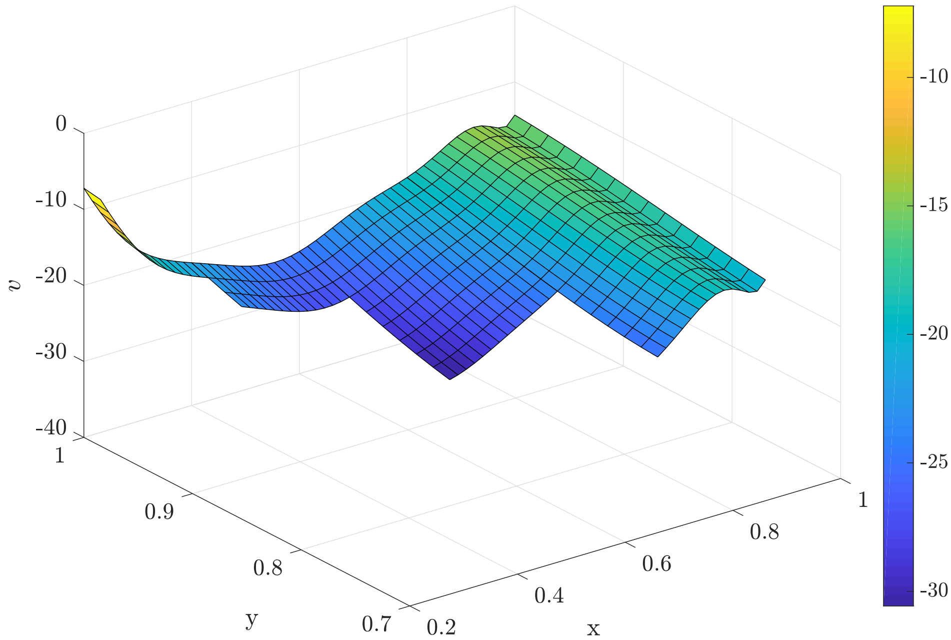

Figure 8: The velocity v of the fluid in Ω_1

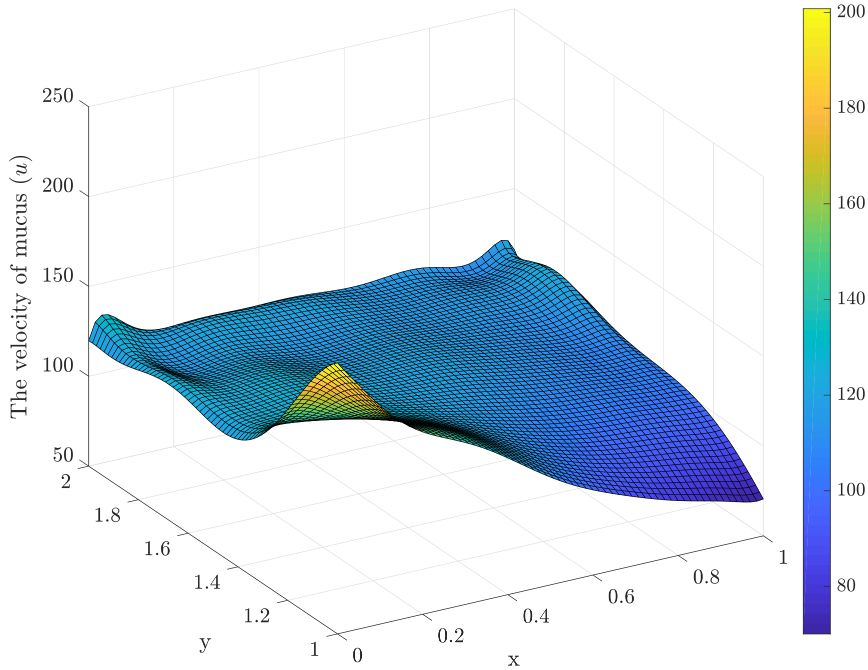

Figure 9: The velocity u of mucus

in Ω_1 and mucus, which are shown in Figure 13. The red asterisk and the blue circle are the speeds of the fluid in Ω_1 and mucus, respectively. The average speed of mucus is about 118 $\mu m/s$ (or about 7.1 mm/min). The curve of the speeds is similar to the average horizontal velocity. It shows the movement of the fluid is possessed by the velocity in x-direction. Next,

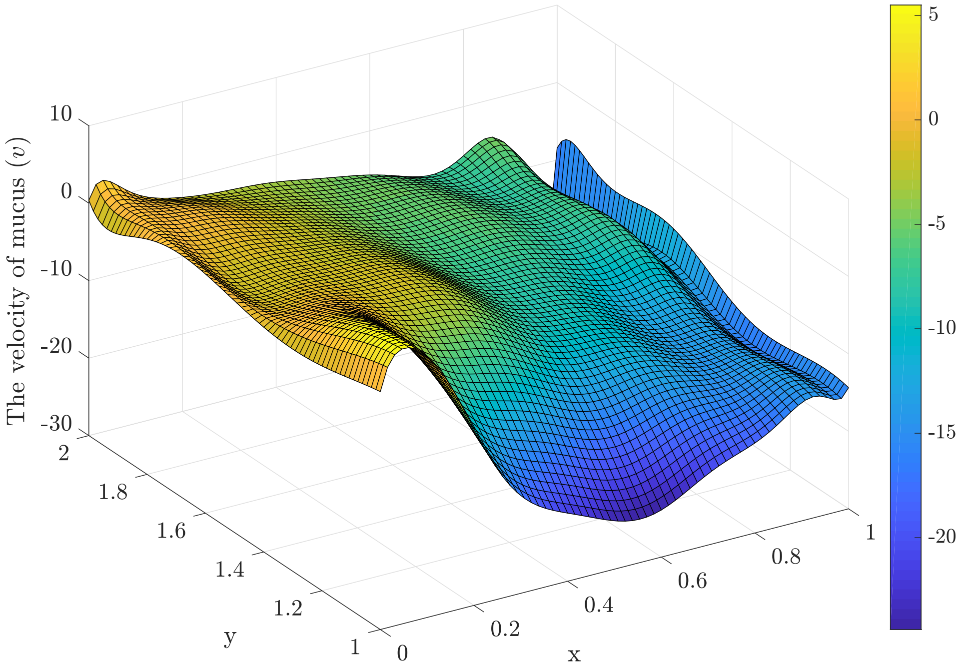

Figure 10: The velocity v of mucus

we compare the average speed of mucus with experimental data in Yeates et al. (1975) in which the mucociliary transport rate has been studied in 42 nonsmoker healthy adults between the ages of 20 to 43 years. The range of the transport rate is $0.8 - 12.4$ mm/min while our result is about 7.1 mm/min. The result is close to the transport rate of men between the ages of $22 - 32$ years and women between the ages of $22 - 30$ years.

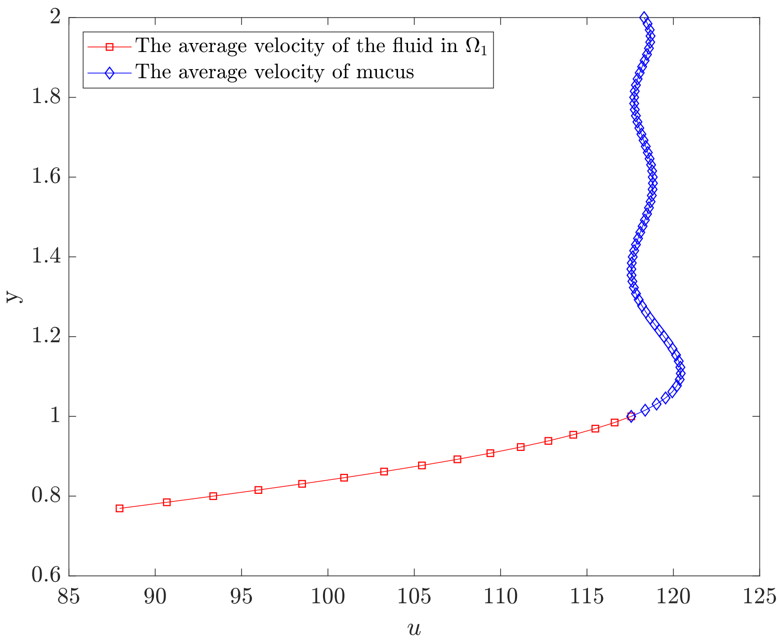

Figure 11: The average velocity u over the $x-$direction of the fluid in Ω_1 and mucus

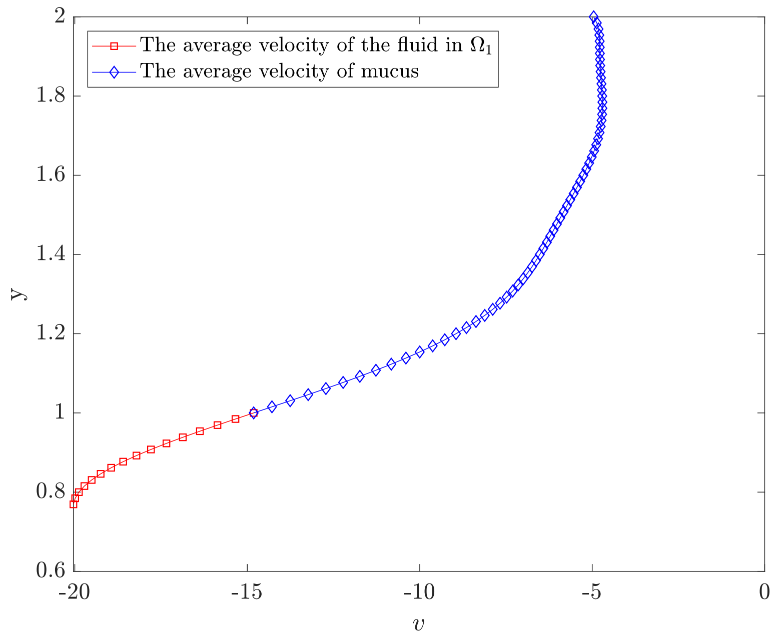

Figure 12: The average velocity v over the $x-$direction of the fluid in Ω_1 and mucus

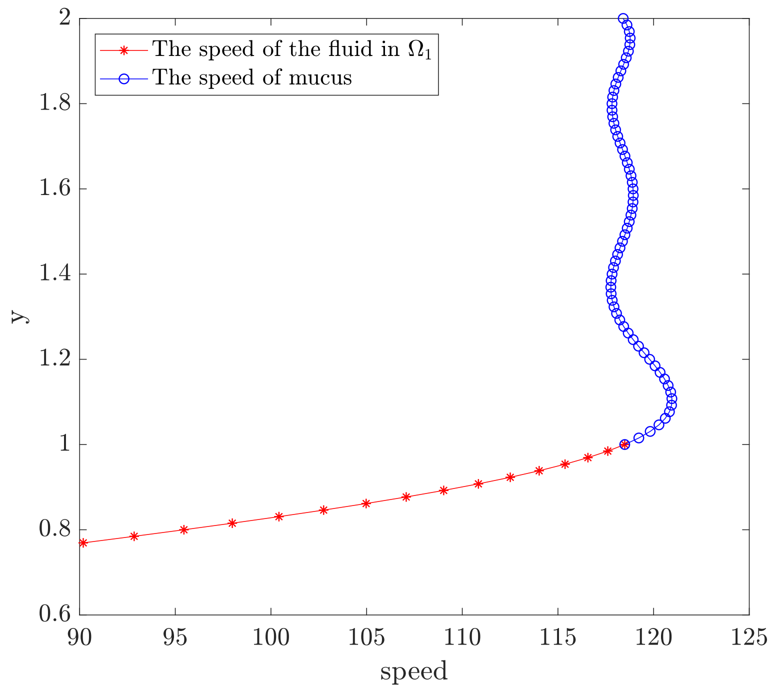

Figure 13: The speeds of the fluid in Ω_1 and mucus

We approximate the speeds of the fluid in Ω_1 and mucus by a polynomial approximation degree 9. The coefficients of the ninth-order polynomial approximation of the speed are shown in Table 2, where h is from $y_{in}(50°)$ to y_{ML}. That is $h = 0.7660$ to $h = 2$. Figure 14 displays the polynomial approximation with the fluid speed in Ω_1 and Ω_2, where the green square, the red asterisk and the blue circle refer to the polynomial approximation, the speed of the fluid in Ω_1 and the speed of mucus, respectively. It shows that the polynomial approximation estimates the speeds of the fluid in Ω_1 and mucus well with the l_2-norm error 0.0282.

Table 2: The ninth-order polynomial functions: $p(h) = c_1h^9 + c_2h^8 + c_3h^7 + c_4h^6 + c_5h^5 + c_6h^4 + c_7h^3 + c_8h^2 + c_9h + c_{10}$ for the speeds of the fluid in Ω_1 and mucus.

Coefficient	$10^6\times$
c_1	0.002271511545374
c_2	−0.029497677298672
c_3	0.166716780614724
c_4	−0.537680842522555
c_5	1.089315989130731
c_6	−1.436339487060982
c_7	1.232011089245644
c_8	−0.663157249265035
c_9	0.203717832820274
c_{10}	−0.027239428286010

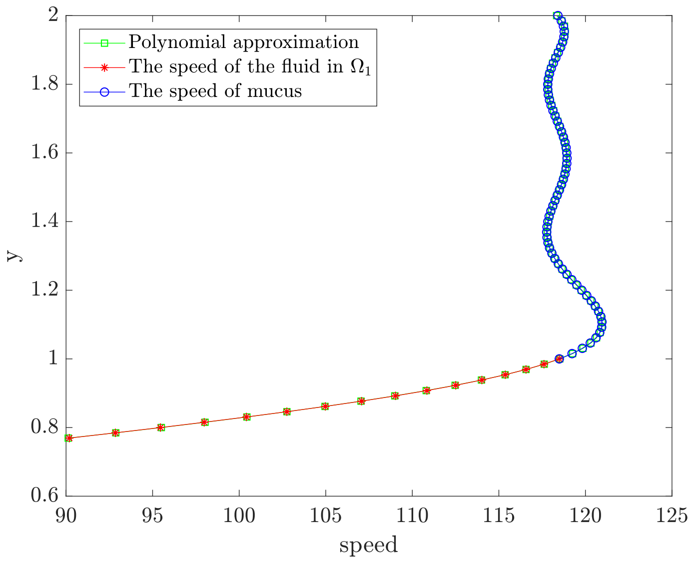

Figure 14: The polynomial approximation and the speeds of the fluid in Ω_1 and mucus

6 Conclusion

In this study, we find the velocity of the fluid in the free-fluid region, Ω_1, and then calculate the mucus velocity in Ω_2. The fluid flows in both domains are affected by cilia movement. We employ the two-dimensional Stokes equation and then apply the mixed finite element method to the equation to calculate the velocities of the fluids in Ω_1 and Ω_2. We first verify the numerical result by averaging our two-dimensional numerical solution over $x-$axis and compare it with the exact solution in the one-dimensional domain in the case of static solid phases. The numerical result converges to the exact solution with the small l_2-norm error.

For the two-dimensional solution, we present the velocity of the PCL fluid in Ω_1 for the angle $\theta = 80^\circ - 50^\circ$ and the mucus velocity. We provide the velocities u and v of the fluid in Ω_1 and then we use them to find the velocity of mucus. The velocities u and v of the fluid in Ω_1 and mucus are averaged over $x-$axis and plotted together in one graph. Next, we find the speed of the average velocities of the fluid in both domains. The shape of the speed is similar to the average velocity u. This indicates that the velocity u has more impact on fluid motion than the velocity v. The speed of the mucus is averaged and compared with the experimental data. Our mucus velocity is about 118 $\mu m/s$ (or about 7.1 mm/min). This result is close to the experimental data of 22- to 32-year-old men and 22- to 30-year-old women (Yeates et al., 1975). The speeds of the fluid in Ω_1 and mucus are approximated by a ninth-order polynomial approximation, provided in Table 2. This work can be effectively applied to problems involving fluid dynamics influenced by the self-movement of solid phases.

Acknowledgement

This paper is supported by the School of Science, King Mongkut's Institute of Technology Ladkrabang, Bangkok, Thailand.

References

Battle, C., Ott, C.M., Burnette, D.T., Lippincott-Schwartz, J. & Schmidt, C.F. (2015). Intracellular and extracellular forces drive primary cilia movement. *Proceedings of the National Academy of Sciences*, *112*(5), 1410–1415.

Boucher, R.C. (1999). Molecular insights into the physiology of the 'thin film' of airway surface liquid. *The Journal of Physiology*, *516*(3), 631-638.

Chamsri, K. (2014). N-dimensional Stokes-Brinkman equations using a mixed finite element method. *Australian Journal of Basic and Applied Sciences*, *8*, 30-36.

Chatelin, R., Poncet, P. (2016). A parametric study of mucociliary transport by numerical simulations of 3D non-homogeneous mucus. *Journal of biomechanics*, *49*(9), 1772–1780.

Derichs, N., Jin, B., Song, Y., Finkbeiner, W.E. & Verkman, A.S. (2011). Hyperviscous airway periciliary and mucous liquid layers in cystic fibrosis measured by confocal fluorescence photobleaching. *The FASEB Journal*, *25*(7), 2325.

Ding, Y., Nawroth, J.C., McFall-Ngai, M.J. & Kanso, E. (2014). Mixing and transport by ciliary carpets: A numerical study. *Journal of Fluid Mechanics*, *743*, 124–140.

Houtmeyers, E., Gosselink, R., Gayan-Ramirez, G. & Decramer, M. (1999). Regulation of mucociliary clearance in health and disease. *European Respiratory Journal*, *13*(5), 1177-1188.

Kasamwan, T., Wuttanachamsri, K. (2020). Unsteady one-dimensional flow in PCL with Stokes-Brinkman equations. *Phayao Research Confernce*, 1949–1964.

Knowles, M.R., Boucher, R.C. (2002). Mucus clearance as a primary innate defense mechanism for mammalian airways. *The Journal of clinical investigation*, *109*(5), 571-577.

Koplik, J., Levine, H. & Zee, A. (1983). Viscosity renormalization in the Brinkman equation. *Physics of Fluids*, *26*, 1958-1988.

Lale, A.M., Mason, J.D.T., & Jones, N.S. (1998). Mucociliary transport and its assessment: A review. *Clinical Otolaryngology & Allied Sciences*, *23*(5), 388-396.

Matthews, L.W., Spector, S., Lemm, J. & Potter, J.L. (1963). Studies on pulmonary secretions: I. The over-all chemical composition of pulmonary secretions from patients with cystic fibrosis, bronchiectasis, and laryngectomy. *American Review of Respiratory Disease*, *88*(2), 199-204.

Modaresi, M.A. & Shirani, E. (2023). Mucociliary clearance affected by mucus-periciliary interface stimulations using analytical solution during cough and sneeze. *The European Physical Journal Plus*, *138*(3), 1-18.

Phaenchat, S., Wuttanachamsri, K. (2019). On the nonlinear Stokes-Brinkman equations for modeling flow in PCL. *The 24th Annual Meeting in Mathematics*, 167-175.

Poopra, S., Wuttanachamsri, K. (2019). The velocity of PCL fluid in human lungs with Beaver and Joseph boundary condition by using asymptotic expansion method. *Mathematics*, *7*(6), 567.

Poopra, S., Wuttanachamsri, K. (2022). On the asymptotic boundary condition at the free-fluid/porous-medium interface in periciliary layer due to the ciliary movement. *Mathematical Problems in Engineering*, *2022*.

Potter, J.L., Matthews, L.W., Spector, S. & Lemm, J. (1967). Studies on pulmonary secretions: II. Osmolality and the ionic environment of pulmonary secretions from patients with cystic fibrosis, bronchiectasis, and laryngectomy. *American Review of Respiratory Disease*, *96*(1), 83-87.

Rusznak, C., Devalia, J.L., Lozewicz, S. & Davies, R.J. (1994). The assessment of nasal mucociliary clearance and the effect of drugs. *Respiratory medicine*, *88*(2), 89-101.

Satir, P., Christensen, S.T. (2007). Overview of structure and function of mammalian cilia. Annu. Rev. Physiol., *69*, 377-400.

Schöberl, J. (1997). NETGEN An advancing front 2D/3D-mesh generator based on abstract rules. *Computing and visualization in science*, *1*(1), 41-52.

Sears, P.R., Thompson, K., Knowles, M.R. & Davis, C.W. (2013). Human airway ciliary dynamics. *American Journal of Physiology-Lung Cellular and Molecular Physiology*, *304*(3), L170-L183.

Sedaghat, M.H., Sadrizadeh, S. & Abouali, O. (2023). Three-dimensional simulation of mucociliary clearance under the ciliary abnormalities. *Journal of Non-Newtonian Fluid Mechanics*, *316*, 105029.

Suankasem, S., Pimkote, A., Thammathon, I. & Wuttanachamsri, K. (2018). Matched asymptotic expansion for PCL fluid due to the movement of lung cilia: part 1. *10th National Science Research Conference*.

The Engineering ToolBox (2003). Water-Density, Specific Weight and Thermal Expansion Coefficients. Retrieved from `https://www.engineeringtoolbox.com/water-density-specific-weight-d_595.html`.

Vanaki, S.M., Holmes, D., Saha, S.C., Chen, J., Brown, R.J. & Jayathilake, P.G. (2020). Mucociliary clearance: A review of modeling techniques. *Journal of Biomechanics*, *99*, 109578.

Verma, V.S. & Rana, V. (2015). Mucus transport in the human lung airways: Effect of porosity parameter and air velocity. *IJSR*, 920-925.

Wanner, A., Salathé, M. & O'Riordan, T.G. (1996). Mucociliary clearance in the airways. *American journal of respiratory and critical care medicine*, *154*(6), 1868-1902.

Wuttanachamsri, K. (2020). Free interfaces at the tips of the cilia in the one-dimensional periciliary layer. *Mathematics*, *8*(11), 1961.

Wuttanachamsri, K., Oangwatcharaparkan, N. & Phaenchat, S. (2024). Wave of Cilia Affecting the Velocity of Fluid in Periciliary Layer. Numerical Algorithms, submitted.

Wuttanachamsri, K. & Schreyer, L. (2020). Effects of cilia movement on fluid velocity: II numerical solutions over a fixed domain. *Transport in Porous Media*, *134*(2), 471-489.

Xu, L., Jiang, Y. (2015). Cilium height difference between Stokes is more effective in driving fluid transport in mucociliary clearance: A numerical study. *Mathematics Biosciences and Engineering*, *12*(5), 1107-1126.

Yeates, D.B., Aspin, N., Levison, H., Jones, M.T. & Bryan, A.C. (1975). Mucociliary tracheal transport rates in man. *Journal of applied physiology*, *39*(3), 487-495.